Efficient robust approximation of the generalised Cornu spiral

Cross, Benjamin; Cripps, Robert J.

DOI:
10.1016/j.cam.2014.05.021

Accepted Manuscript

Efficient robust approximation of the generalised Cornu spiral

Benjamin Cross, Robert J. Cripps

PII: S0377-0427(14)00266-0
DOI: http://dx.doi.org/10.1016/j.cam.2014.05.021
Reference: CAM 9690

To appear in: *Journal of Computational and Applied Mathematics*

Received date: 21 November 2012
Revised date: 29 March 2014

Please cite this article as: B. Cross, R.J. Cripps, Efficient robust approximation of the generalised Cornu spiral, *Journal of Computational and Applied Mathematics* (2014), http://dx.doi.org/10.1016/j.cam.2014.05.021

Efficient Robust Approximation of the Generalised Cornu Spiral

Benjamin Cross and Robert J. Cripps

Geometric Modelling Group, School of Mechanical Engineering,
University of Birmingham, Birmingham, B15 2TT, UK

Abstract

A Generalised Cornu Spiral (GCS) is a planar curve defined to have a monotonic rational linear curvature profile and as such these curves are considered fair. However, their implementation in current CAD systems is not straight forward partly due to not being in the usual polynomial form. A GCS cannot be expressed exactly using a finite polynomial and so a compromise can be achieved by instead approximating the GCS with a suitable polynomial.

An efficient robust approximation of the GCS using quintic polynomials is presented. The approximation satisfies the G^2 continuity conditions at the end points and the remaining four degrees of freedom are argued for by looking at G^3 approximations. The method begins by reparamterising the GCS in terms of more intuitive geometric descriptions; the winding angle, change in curvature and a shape factor. The G^3 approximations provide insight to help define values for the free parameters, and the new geometric form allows for the shortcomings in the G^3 approximations to be controlled.

The efficiency of the approximation is improved compared to earlier methods which required a numerical search. Also, there is strong evidence that the method guarantees a satisfactory approximation when the GCS lies within certain identified bounds.

1 Introduction

A Generalised Cornu Spiral (GCS) is a planar curve defined to have a monotonic rational linear curvature profile [1] and as such these curves are considered fair [2]. Fair curves are useful within CAD, as they provide the

aesthetics designers require [3]. Controlling curvature, as the second derivative with respect to (w.r.t.) arc length, has practical uses corresponding to physical properties; such as unilateral force experienced when travelling on a path with constant speed. GCS curves are therefore useful in span generation such as transition curves between two data points [1]. This is particularly true for the Cornu spiral, which is itself a member of the GCS family, having applications in highway design, robotics and roller coaster design [4] [5].

In order to utilise a GCS curve within CAD the coordinates for an arbitrary point must be calculated. These points are found by first integrating the curvature, then integrating these functions from within the sin/cos functions, both w.r.t. arc length, allowing for initial conditions. These integrals contain non-fundamental functions, such as the Fresnel integrals in the case of the Cornu sprial, and thus are usually obtained by numerical integration [1]. As a consequence this representation is impractical for direct use within CAD.

A more widely used representation for CAD based curves is a polynomial, such as a B-spline or a Bézier curve. The problem with these representations is that the curvature is hard to control and hence fairness is difficult to obtain [8]. A GCS cannot be expressed exactly using a finite polynomial [7] and so a compromise can be achieved by instead approximating the GCS with a suitable polynomial.

The best approximations should mimic the property of rational linear curvature. This suggests that rather than using traditional measures of error, such as Hausdorff distance, the curvature profiles of the GCS and the approximation should be compared; as proposed in [9].

A well known approximation method uses the Hermite spline [15] which interpolates start and end k^{th} derivative data with the unique polynomial of order $(2k + 1)$. However, in order to obtain a satisfactory approximation, k may be too large for practical use.

A different approach was proposed in [9] wherein the degree of the polynomial was restricted to quintic. Position, tangent direction and curvature values were interpolated at the start and end points leaving four degrees of freedom. These four parameters were then varied in a search until the approximation was deemed satisfactory. This occurred when the relative curvature difference between the curves was less than some tolerance.

A similar approach was taken in [10] also using quintic curves. Two free parameters from the Hermite approximation, relating to end tangent magnitudes, were discovered. Values for these parameters were then determined by minimising the energy, that is the integral of the curvature squared w.r.t. arc length, using an optimisation procedure. The problem with both of these techniques is that the numerical search and the optimisation procedure are

computationally expensive. Each configuration required the quintic polynomial to be reparameterised with respect to arc length to enable comparison of curvature values or energy.

The method of [9] was improved in [8] by insisting that the start and end points obey the G^3 constraints reducing the degrees of freedom from four to two. Approximations are formed using initial values, corresponding to matching end tangent magnitudes, and often produce satisfactory approximations. However, when the initial values for these parameters produce unsatisfactory approximations, different values are determined using a numerical search. The reduced degrees of freedom as well as understanding of the search domain produces a search routine more efficient than the one in [9].

A weakness of the approximation techniques in [9], [10] and [8] is that they are *non-deterministic* in the sense that they require a numerical search. Any search based solutions raise concerns with efficiency and robustness. They can be considered inefficient as they consume relatively large computational overheads. Furthermore, it is not possible to guarantee that after performing these computations a satisfactory solution will be found. For this reason they cannot be considered robust. This paper addresses these concerns by presenting a method such that given suitable bounds on a GCS, an acceptable approximation can be found without the need for a search.

It is the intention of this research to eventually be able to produce an efficient polynomial curve construction algorithm that yields curves with high-quality shape characteristics based upon geometric data. While other high-quality curves described directly via their curvature profile do exist, such as polynomial functions of arc-length [12], deterministic algorithms to convert these curves into a polynomial form do not. Furthermore, the GCS is considered a suitable candidate from this family since existing research has already shown that a GCS can be fitted to G^2 data within a reasonable tolerance [1]. An initial approach would be to fit a GCS to some data and then form the polynomial approximation. This process of finding the GCS satisfying given geometric data is currently a numerically expensive process. However, it may be possible to *reverse engineer* the GCS approximation from the data without having to find the specific GCS. This idea is discussed in more detail in the conclusion.

In the next two sections some background information and preliminaries are discussed. Using this information an approximation method is described in section four. Analysis and examples are discussed in section five and six respectively which is then followed in section seven by some concluding remarks including possible improvements and future research.

2 Background Information

2.1 The GCS

GCS curves are defined to have a rational linear monotonic curvature profile. Explicitly, the curvature profile of a GCS has the form:

$$\kappa(s) = \frac{\kappa_0 S + (\kappa_1 - \kappa_0 + r\kappa_1)s}{S + rs} \qquad s \in [0, S],\ r \in (-1, \infty), \tag{1}$$

where the parameter s represents the arc length of the curve, κ_0 and κ_1 represent the start and end curvature values respectively, S corresponds to the length of the GCS and r, $(r > -1)$, is referred to as the shape factor.

The curvature profile however, only describes the shape of the curve. Translations or rotations do not affect the curvature. Therefore, in order to completely define the curve in $\mathbb{R}^2$, its initial location, (x_0, y_0), and orientation, θ_0, must be defined [13]. The orientation is decided by the angle, θ_0, that the initial tangent vector makes with the positive x-axis.

Scaling of the curve can also be accounted for. Applying a scaling factor λ, new values for the parameters can be calculated as: $S^* = \lambda S$, $\kappa_0^* = \frac{\kappa_0}{\lambda}$, $\kappa_1^* = \frac{\kappa_1}{\lambda}$ and $r^* = r$ [13].

Thus given a GCS, it is always possible to express it in *normal form*. This is achieved by firstly translating the GCS to the origin (i.e. setting $x_0 = 0, y_0 = 0$). The curve is then rotated so that the initial tangent is in the direction of the positive x-axis ($\theta_0 = 0$). Finally the curve is scaled to make the arc length equal to 1.

A normalised GCS is therefore completely defined by the triplet $\{\kappa_0, \kappa_1, r\}$ and for the purposes of this paper all future GCS curves are considered to be in normal form.

The GCS curve can be synthesised parametrically from [1]:

$$\mathbf{F}(t) = \begin{bmatrix} x(t) \\ y(t) \end{bmatrix} = \begin{bmatrix} x_0 + \int_0^t \cos\left[\theta_0 + \int_0^\sigma \kappa(s)ds\right]d\sigma \\ y_0 + \int_0^t \sin\left[\theta_0 + \int_0^\sigma \kappa(s)ds\right]d\sigma \end{bmatrix} \tag{2}$$

$$= \begin{bmatrix} \int_0^t \cos\left[\int_0^\sigma \frac{\kappa_0 + (\kappa_1 - \kappa_0 + r\kappa_1)s}{1 + rs}ds\right]d\sigma \\ \int_0^t \sin\left[\int_0^\sigma \frac{\kappa_0 + (\kappa_1 - \kappa_0 + r\kappa_1)s}{1 + rs}ds\right]d\sigma \end{bmatrix}.$$

Then if $r = 0$:

$$\begin{bmatrix} x(t) \\ y(t) \end{bmatrix} = \begin{bmatrix} \int_0^t \cos\left[\kappa_0\sigma + \frac{1}{2}(\kappa_1 - \kappa_0)\sigma^2\right]d\sigma \\ \int_0^t \sin\left[\kappa_0\sigma + \frac{1}{2}(\kappa_1 - \kappa_0)\sigma^2\right]d\sigma \end{bmatrix},$$

otherwise:

$$\begin{bmatrix} x(t) \\ y(t) \end{bmatrix} = \begin{bmatrix} \int_0^t \cos\left[\frac{r((1+r)\kappa_1 - \kappa_0)\sigma + (1+r)(\kappa_0 - \kappa_1)ln(1+r\sigma)}{r^2}\right]d\sigma \\ \int_0^t \sin\left[\frac{r((1+r)\kappa_1 - \kappa_0)\sigma + (1+r)(\kappa_0 - \kappa_1)ln(1+r\sigma)}{r^2}\right]d\sigma \end{bmatrix}.$$

The derivative information at the start and end points can thus be calculated as:

$$\begin{aligned}
\mathbf{F}(0) =& (0,0) & \mathbf{F}(1) =& (x,y) \\
\mathbf{F}'(0) =& (1,0) & \mathbf{F}'(1) =& (\cos\theta, \sin\theta) \\
\mathbf{F}''(0) =& (0,\kappa_0) & \mathbf{F}''(1) =& \kappa_1(-\sin\theta, \cos\theta) \\
\mathbf{F}'''(0) =& \mathbf{F}''(0)\frac{\kappa'(0)}{\kappa(0)} - \mathbf{F}'(0)\kappa(0)^2 & \mathbf{F}'''(1) =& \mathbf{F}''(1)\frac{\kappa'(1)}{\kappa(1)} - \mathbf{F}'(1)\kappa(1)^2 \\
=& (-\kappa_0^2, (\kappa_1 - \kappa_0)(1+r)) & =& \mathbf{F}''(1)\frac{(\kappa_1 - \kappa_0)}{\kappa_1(1+r)} - \mathbf{F}'(1)\kappa_1^2
\end{aligned}$$

where $'$ represents differentiation w.r.t. the parameter t, (x, y) is the end point and θ is the winding angle calculated from:

$$\theta = \int_0^1 \kappa(s)ds = \int_0^1 \frac{(\kappa_1 - \kappa_0 + r\kappa_1)s + \kappa_0}{rs+1}ds \tag{3}$$

$$= \begin{cases} \dfrac{\kappa_0 + \kappa_1}{2} & \text{if } r = 0, \\ \dfrac{r(\kappa_1(1+r) - \kappa_0) + (1+r)(\kappa_0 - \kappa_1)ln(1+r)}{r^2} & r \neq 0. \end{cases}$$

It is noted that

$$\kappa'(s) = \frac{d}{ds}\left(\frac{(\kappa_1 - \kappa_0 + r\kappa_1)s + \kappa_0}{rs+1}\right) = \frac{(\kappa_1 - \kappa_0)(1+r)}{(rs+1)^2}$$

and

$$\kappa'(0) = (\kappa_1 - \kappa_0)(1+r) \qquad \kappa'(1) = \frac{(\kappa_1 - \kappa_0)}{(1+r)}$$

The end point can be calculated by numerical integration of (2), using for example Romberg integration [16].

2.2 A G^3 construction

In [8] a quintic Bézier approximation that matches G^3 conditions at the start and end points is described. Two free parameters (β_1, γ_1), relating to the size of the start and end tangent magnitudes respectively, are used to define an approximation. These parameters are called *shape factors* [17] and are associated with the approximation and are not to be confused with the shape factor r of the GCS.

The G^3 approximation [8] is found by setting the control vertices to:

$$\begin{aligned}
\mathbf{V}_0 &= \mathbf{F}(0) \\
\mathbf{V}_1 &= \frac{\beta_1}{5}\mathbf{F}'(0) + \mathbf{F}(0) \\
\mathbf{V}_2 &= \frac{\beta_1^2}{20}\mathbf{F}''(0) + \big(\frac{\beta_2}{20} + \frac{2\beta_1}{5}\big)\mathbf{F}'(0) + \mathbf{F}(0) \\
\mathbf{V}_3 &= \frac{\gamma_1^2}{20}\mathbf{F}''(1) + \big(\frac{\gamma_2}{20} - \frac{2\gamma_1}{5}\big)\mathbf{F}'(1) + \mathbf{F}(1) \\
\mathbf{V}_4 &= \frac{-\gamma_1}{5}\mathbf{F}'(1) + \mathbf{F}(1) \\
\mathbf{V}_5 &= \mathbf{F}(1).
\end{aligned} \tag{4}$$

where β_2 and γ_2 are dependent on β_1 and γ_1.

The two supplementary values β_2, γ_2 are the second shape factors for the approximation and are calculated by:

$$\beta_2 = \frac{B(\beta_1, \gamma_1)}{D(\beta_1, \gamma_1)} \qquad \& \qquad \gamma_2 = \frac{G(\beta_1, \gamma_1)}{D(\beta_1, \gamma_1)} \tag{5}$$

where,

$$\begin{aligned}
B(\beta_1, \gamma_1) = \big(&60x - 24\beta_1 + 24\cos(\theta)^2\beta_1(1+r) - 60\cos(\theta)^2 x(1+r) \\
&- 3\cos(\theta)\kappa_1^2\gamma_1^3 + \beta_1^3\kappa_1^2\gamma_1 - 60y\kappa_1\gamma_1(1+r) + 9\kappa_0\beta_1^2\kappa_1\gamma_1 \\
&- 60\sin(\theta)\cos(\theta)y(1+r) + 3\kappa_0\sin(\theta)\cos(\theta)\beta_1^2(1+r) \\
&+ 2\beta_1^3\kappa_1^2\gamma_1 r + \beta_1^3\kappa_1^2\gamma_1 r^2 - \beta_1^3\kappa_1\gamma_1\kappa_0 - 24\beta_1 r - 3\gamma_1^3\cos(\theta)\kappa_1^2 r \\
&+ 60xr - 9\kappa_0\beta_1^2\kappa_1\gamma_1 r - 2\beta_1^3\kappa_1\gamma_1\kappa_0 r - \beta_1^3\kappa_1\gamma_1\kappa_0 r^2 \\
&+ 15\sin(\theta)\kappa_1\gamma_1^2(1+r) + \sin(\theta)\gamma_1^3(\kappa_1 - \kappa_0) \\
&+ 9\cos^2(\theta)\sin(\theta)\kappa_1\gamma_1(1-\gamma_1)(1+r)\big)/(-3(1+r)).
\end{aligned}$$

$$
\begin{aligned}
G(\beta_1,\gamma_1) =& \big(24\gamma_1(1+r) - 60\sin(\theta)y(1+r) + 3\cos(\theta)\kappa_0^2\beta_1^3(1+r) \\
&- 15\sin(\theta)\kappa_0\beta_1^2(1+r) - 60\cos(\theta)y\beta_1\kappa_0(1+r) \\
&- 3\sin(\theta)\cos(\theta)\kappa_1\gamma_1^2(1+r) - \sin(\theta)\beta_1^3\kappa_0 + \sin(\theta)\beta_1^3\kappa_1 \\
&+ 2\sin(\theta)\beta_1^3\kappa_1 r + \sin(\theta)\beta_1^3\kappa_1 r^2 + 60x\sin(\theta)\beta_1\kappa_0(1+r) \\
&- 2\sin(\theta)\beta_1^3\kappa_0 r - \sin(\theta)\beta_1^3\kappa_0 r^2 + \gamma_1^3\beta_1\kappa_0\kappa_1 - \gamma_1^3\beta_1\kappa_0^2 \\
&- 9\kappa_1\gamma_1^2\beta_1\kappa_0(1+r) - 24\cos(\theta)^2\gamma_1(1+r) \\
&+ 9\cos^2(\theta)\kappa_0\kappa_1\beta_1\gamma_1(1-\gamma_1)(1+r)\big)/(-3(1+r)).
\end{aligned}
$$

$$
D(\beta_1,\gamma_1) = \beta_1\gamma_1\kappa_0\kappa_1 - \sin^2(\theta).
$$

Thus, given values for shape factors (β_1, γ_1) a G^3 approximation to a GCS is possible. The method in [8] assigns initial values of 1 to both the shape factors so to match the end tangent magnitudes with the GCS representation. If this approximation does not suffice then a search is performed on the two parameters (β_1, γ_1) via Powell's method [16]. A search was shown to be necessary when the denominator function, $D(\beta_1, \gamma_1)$, approaches zero causing a divergence of the shape factors (β_2, γ_2) [8].

2.3 Measuring the error

The defining property of the GCS is its rational monotonic curvature profile. An approximation to a GCS should therefore mimic this behavior. Thus the error of an approximation should ideally be based on its curvature.

In [8] an error function, ϵ, was defined as the minimum of two functions; the absolute curvature difference and the relative curvature difference. In order to compare the curvature values the Bézier curve was reparamaterised w.r.t. arc length and scaled to limit the domain to $[0, 1]$. The maximumum error throughout the domain was taken as the error ϵ:

$$
\epsilon = \epsilon(\kappa_b, \kappa_g) = \max_{s\in[0,1]} \frac{|\kappa_b(s) - \kappa_g(s)|}{\max\{|\kappa_g(s)|, 1\}}.
$$

where $\kappa_g(s)$ is the curvature of the GCS and $\kappa_b(s)$ is the curvature of the reparameterised Bézier.

An approximation is considered acceptable if the error is within some tolerance i.e. $\epsilon \leq \mu$. A tolerance of $\mu = 0.05$ ensures that a curve is of high quality [1] [18] and thus any curve that satisfies $\epsilon \leq 0.05$ is deemed an acceptable approximation.

The continuity of this function is briefly discussed here to aid the analysis in section 5. Since the function is defined as the minimum of two C^0 continuous functions, ϵ is also C^0 continuous. Furthermore, C^1 continuity can not be guaranteed if there exists $s_1, s_2 \in (0,1)$ such that $|\kappa_g(s_1)| < 1$ and $|\kappa_g(s_2)| > 1$. A consequence of this is that the derivatives of ϵ are intractable.

3 Preliminaries

Recall the form for a GCS's curvature from (1). The winding angle of the GCS, θ, can be calculated from (3). Rearranging this equation the winding angle, θ, can be shown to be a convex combination of the start and end curvatures κ_0 and κ_1, i.e.

$$\theta = m(r)\kappa_0 + (1 - m(r))\kappa_1$$

where,

$$m(r) = \begin{cases} \frac{1}{2} & \text{if } r = 0, \\ \dfrac{(1+r)\ln(1+r) - r}{r^2} & r \neq 0. \end{cases}$$

It is shown in [1] that $m(r)$ is a monotonic function that lies in $(0,1)$ and therefore the winding angle, θ, lies between κ_0 and κ_1.

3.1 Reparameterising the shape factor

The shape factor r lies in the range $(-1, \infty)$. To aid the algebra and for analysis purposes a rational linear transformation is applied to r such that

$$r(u) = \frac{1-2u}{u-1} \quad \Rightarrow \quad u(r) = \frac{r+1}{r+2} \tag{6}$$

so that the domain of u lies in the finite range $(0,1)$. It is worth noting that this reparameterisation does not affect the curvature profile and thus the shape of the curve. The parameter u is referred to as the *modified shape factor*.

The winding angle can then be expressed as:

$$\begin{aligned} \theta &= m(u(r))\kappa_0 + (1 - m(u(r)))\kappa_1 \\ &= \lambda(u)\kappa_0 + (1 - \lambda(u))\kappa_1 \\ &= \lambda\kappa_0 + (1-\lambda)\kappa_1 \end{aligned} \tag{7}$$

where,

$$\lambda(u) = \begin{cases} \frac{1}{2} & \text{if } u = \frac{1}{2}, \\ \dfrac{1-u}{2u-1}\left(\dfrac{u}{2u-1}\ln\left(\dfrac{u}{1-u}\right) - 1\right) & u \neq \frac{1}{2}. \end{cases}$$

3.2 A GCS class

Poor approximations in [8] were attributed to the divergent behaviour of the shape factors β_2, γ_2. This was caused by zero-values for the denominator function, $D(\beta_1, \gamma_1)$ (4). Analysing the denominator value,

$$D(\beta_1, \gamma_1) = \beta_1\gamma_1\kappa_0\kappa_1 - \sin^2(\theta),$$

can help determine any divergent behaviour.

One possible technique to reduce the complexity of the zero-denominator issue is to only consider a one parameter variation of a GCS at a time. This is the motivation for creating a *GCS class*. By establishing the denominator values within a single-parameter class, zeros can be identified easily.

Recall that the set of (normalised) GCSs is defined by 3 parameters $\{\kappa_0, \kappa_1, r\}$. To create a 1-parameter family of curves an invariance of two independent parameters must be inherited by every class. In theory, any two of $\{\kappa_0, \kappa_1, r\}$ could be chosen. However to reduce the complexity a different invariance is considered, an invariance on the winding angle, θ. Not only does this provide a geometric description but it also keeps the second term in $D(\beta_1, \gamma_1)$ constant. The second invariance to be enforced on each class is chosen to be u (equivalently r).

Insisting on this invariance, the set of GCS curves are partitioned into classes wherein each curve shares the same winding angle, θ, and modified shape factor, u. These classes are denoted as $\mathcal{C}_{u,\theta}$ with each member $\mathcal{C}_{u,\theta}(t)$ defined by

$$\begin{aligned} \kappa_0 &= \theta + (1 - \lambda(u))t \\ \kappa_1 &= \theta - \lambda(u)t \\ r &= \frac{1-2u}{u-1}. \end{aligned}$$

It can easily be verified by substitution into (6) and (7) that each member of the class has winding angle θ and modified shape factor u. Thus varying the parameter t will not affect θ or u. Furthermore,

$$t = \kappa_0 - \kappa_1. \tag{8}$$

By assuming that the shape factors β_1 and γ_1 do not vary within a class, a point which is justified in the next section, the distribution of the denominator $D(\beta_1, \gamma_1; t)$ within a class is shown to be:

$$\begin{aligned} D(t) =& \beta_1\gamma_1(\theta + (1-\lambda(u))t)(\theta - \lambda(u)t) - \sin^2(\theta) \\ =& \beta_1\gamma_1\theta^2 - \sin^2(\theta) + \beta_1\gamma_1\theta(1-2\lambda)t - \beta_1\gamma_1(1-\lambda)\lambda t^2. \end{aligned}$$

The distribution is quadratic w.r.t t and thus the zeros of $D(t)$ occur when

$$t = t_0 \pm d = \frac{\theta(1-2\lambda)}{2(1-\lambda)\lambda} \pm \frac{\sqrt{\beta_1\gamma_1\theta^2 - 4(1-\lambda)\lambda\sin^2(\theta)}}{\sqrt{\beta_1\gamma_1}2(1-\lambda)\lambda}. \tag{9}$$

By changing the defining parameters of a GCS to the triplet $\{\theta, t, u\}$ a new spanning set is formed. Properties of these parameters are now discussed to help determine suitable bounds for an approximation.

3.3 Establishing bounds for the GCS

To begin, equivalence relationships between the new set of parameters can be shown by symmetry. Enforcing an approximation to also behave symmetrically reduces the overall range of parameter values that need to be considered.

Using symmetrical arguments, any GCS with a negative winding angle, $\mathcal{C}_{u,-\theta}(t)$, is equivalent to the curve with positive winding angle $\mathcal{C}_{u,\theta}(-t)$ but reflected in the x-axis. Similarly, for a curve with a negative parameter for t (i.e. $\kappa_0 < \kappa_1$) $\mathcal{C}_{u,\theta}(-t)$ corresponds to a reflection in the curvature profile to $\mathcal{C}_{1-u,\theta}(t)$. Thus the two curves are reflections of each other. Therefore when considering the set of GCS curves it is reasonable to assume that $t, \theta \geq 0$.

Although approximations can be formed for any values for $\{\theta, u, t\}$, restrictions on the input parameters are often made to ensure high quality approximations [1] [9] [14]. For example, the winding angle in practical road design is restricted to $|\theta| \leq \frac{\pi}{2}$ [14]. Similarly in [9], the winding angle is restricted to $|\theta| \leq \frac{\pi}{2}$ which was arrived at empirically. In [1], when creating a practical solution to span generation using GCS curves, the shape factor is restricted so that $|m(r) - \frac{1}{2}| < 0.4$.

The following bounds for $\{\theta, u, t\}$ were arrived at using existing restrictions and empirical evidence. The winding angle is restricted to $|\theta| \leq \frac{\pi}{2}$, the shape factor u is bounded by $|u - \frac{1}{2}| \leq 0.4$ and t limited to $|t| \leq \pi$. The winding angle restriction agrees with bounds from [14] and [9]. The bounds on u and t were arrived at as a result of observations with the intention of maximising the region of admissible values.

By imposing the symmetry, a final bounding set of $\mathbf{D} = \{(\theta, t, u) : \theta \in [0, \frac{\pi}{2}], t \in [0, \pi], u \in [0.1, 0.9]\}$ is equivalent to the GCSs satisfying the bounds $|\theta| \leq \frac{\pi}{2}$, $|u - \frac{1}{2}| \leq 0.4$ and $|t| \leq \pi$.

4 Method

In section 2.2, a G^3 approximation to a GCS was formed given shape factors (β_1, γ_1). To find suitable values for the two shape factors a numerical search can be used, such as [8], at a high computational expense. Given suitable values, acceptable approximations can be found without the need for a search much faster.

In order to gain insight suitable values of (β_1, γ_1) given $\{\theta, u, t\}$ could be established. However, there is generally a region of sufficient values (should they exist) corresponding to acceptable approximations. Instead unique values for the shape factors are considered. These unique values are calculated by performing a search on (β_1, γ_1) as outlined in [8] until a local minimum is found. Although this may not be the global minimum and thus the true optimum value, the values still provide enough insight to determine a relationship with the GCS.

Within the set of GCS curves with $t \in [0, \pi]$, $u \in (0, 1)$ at bounding planes $\theta = 0, \frac{\pi}{2}$ a search for (β_1, γ_1) values was performed. The findings are illustrated in Figures 1-3. Figure 1 shows the accuracy for each GCS approximation while Figures 2 and 3 show the values of β_1 and γ_1 respectively.

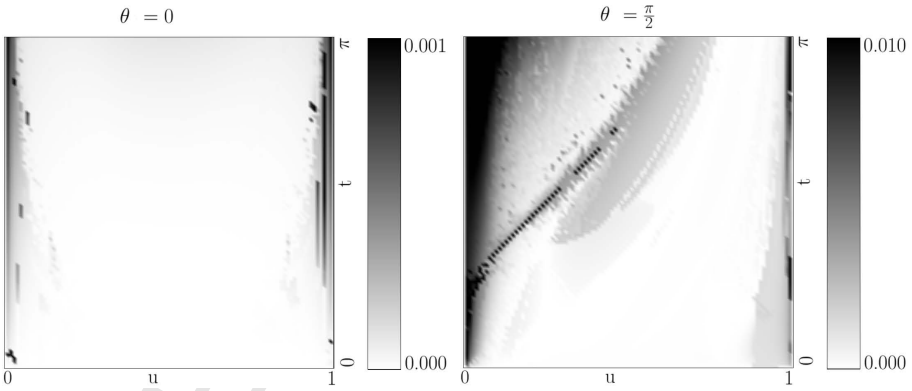

Figure 1: ϵ values from a G^3 search: $u \in (0, 1), t \in [0, \pi]$ for $\theta = 0$ (left) and $\theta = \frac{\pi}{2}$ (right).

Noisy data can be attributed to the instability of the denominator $D(\beta_1, \gamma_1)$ coupled with the numerical approach. As expected, when $\theta = \frac{\pi}{2}$ the search

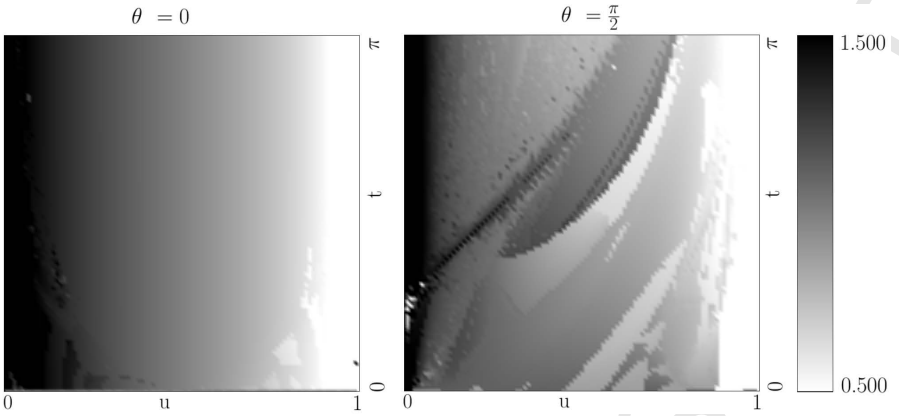

Figure 2: β_1 values from a G^3 search: $u \in (0,1), t \in [0,\pi]$ for $\theta = 0$ (left) and $\theta = \frac{\pi}{2}$ (right).

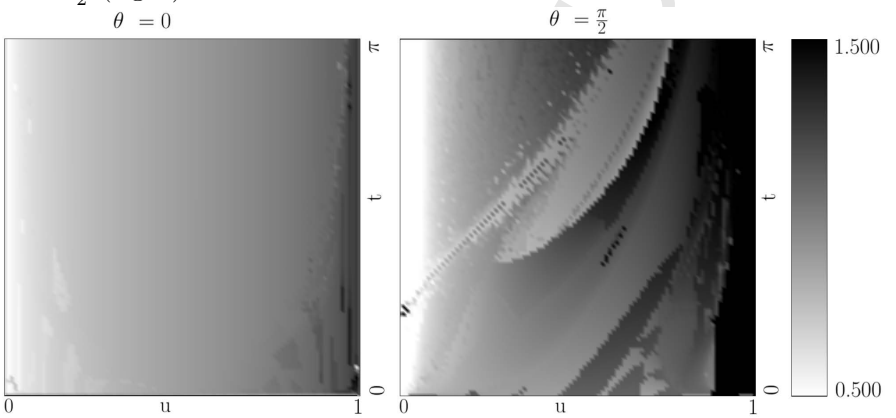

Figure 3: γ_1 values from a G^3 search: $u \in (0,1), t \in [0,\pi]$ for $\theta = 0$ (left) and $\theta = \frac{\pi}{2}$ (right).

is less stable and produces poorer approximations. Another observation to note is that as $u \to 0, 1$ the quality of the approximations deteriorate as a consequence of the divergent behaviour at $u = 0, 1$. This verifies that a bound on u is necessary.

The distribution of the shape factors, as shown in Figures 2 and 3, provide important insight. Firstly, notice that as t varies, i.e. the vertical segments of the graph, the shape factors do not vary too much (within the stable regions). This supports the proposition that the shape factors should be invariant in t as assumed in section 3.2. Furthermore, ignoring the effect of the noisy data with $\theta = \frac{\pi}{2}$, the adjacent graphs in figures 2 and 3 closely resemble

each other. This supports the assumption that β_1 and γ_1 do not have to be dependent upon θ.

Secondly, notice how the shape parameters β_1 and γ_1 vary with the modified shape factor u. A simple way to imitate this relationship is to apply a linear approximation. This approximation is chosen to be

$$\beta_1(u) = 1.5 - u, \quad \gamma_1(u) = 0.5 + u. \tag{10}$$

The property that $\beta_1(u) = \gamma_1(1-u)$ guarantees approximations to symmetrical GCSs are equivalent, a requirement discussed in section 3.3.

G^3 approximations can be performed given the newly defined values for (β_1, γ_1). When the denominator $D(\beta_1, \gamma_1)$ approaches zero, and hence the second shape factors (β_2, γ_2) diverge, poor approximations still occur. By considering the distribution of these second shape factors for a GCS class, divergent regions are identified to occur at the values $t = t_0 \pm d$ given (9).

Taking Figure 4 as an example of a second shape factors' distribution within a class, away from divergent regions the distribution is approximately linear. Imposing this linear distribution around the divergent regions will provide stability.

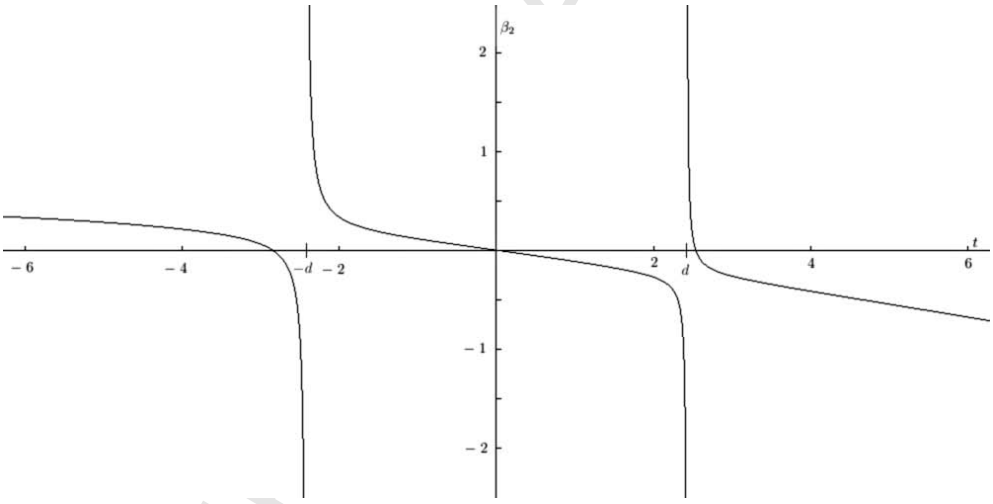

Figure 4: β_2 values for $\mathcal{C}_{0,\frac{\pi}{2}}(t)$. Divergence occurs local to $t = t_0 \pm d = 0 \pm \frac{\sqrt{(\frac{\pi}{2})^2 - 1}}{2}$.

A linear interpolation, symmetric about the two divergent points is created. Let the β_2 values at $t = t_0 - 2d, t_0, t_0 + 2d$, derived from (5), be denoted by b_{-1}, b_0, b_1 respectively. Then the linear interpolation is defined

by the following equation (see Figure 5).

$$\beta_2(t) = \begin{cases} b_0 + \frac{t_0 - t}{2d}(b_{-1} - b_0) & \text{if } t \in (t_0 - 2d, t_0) \\ b_0 + \frac{t_0 - t}{2d}(b_1 - b_0) & \text{if } t \in (t_0, t_0 + 2d) \\ \beta_2(\frac{1}{2} + u, \frac{3}{2} - u) & \text{otherwise.} \end{cases} \tag{11}$$

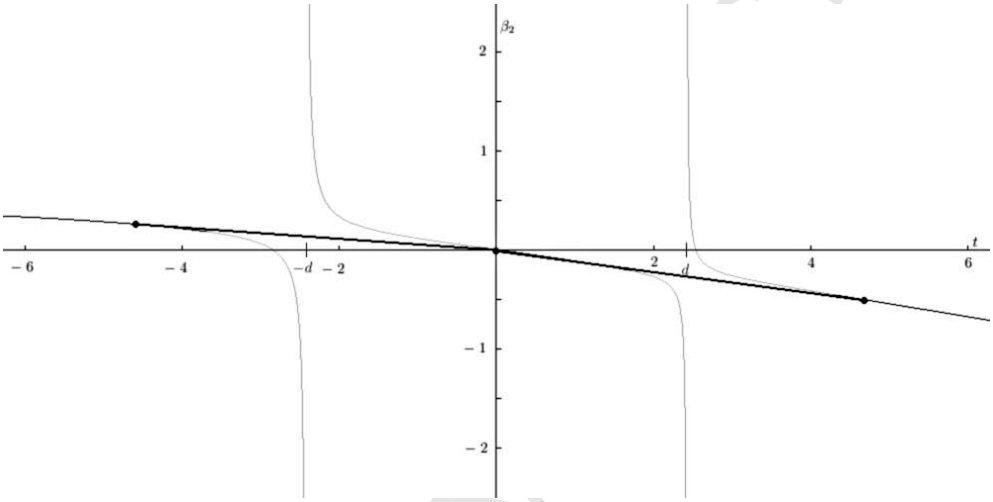

Figure 5: β_2 values for $\mathcal{C}_{0,\frac{\pi}{2}}(t)$ linearly interpolated across $t = t_0 - 2d, t_0, t_0 + 2d$.

Similarly, a linear interpolation of the γ_2 values in a class is created. Let the γ_2 values at $t = t_0 - 2d, t_0, t_0 + 2d$ be denoted by g_{-1}, g_0, g_1 respectively. Then

$$\gamma_2(t) = \begin{cases} g_0 + \frac{t_0 - t}{2d}(g_{-1} - g_0) & \text{if } t \in (t_0 - 2d, t_0) \\ g_0 + \frac{t_0 - t}{2d}(g_1 - g_0) & \text{if } t \in (t_0, t_0 + 2d) \\ \gamma_2(\frac{1}{2} + u, \frac{3}{2} - u) & \text{otherwise.} \end{cases} \tag{12}$$

Defining the values of the second shape factors (β_2, γ_2) in this way prevents divergent behaviour and gives C^0 continuity for the distribution of these values whenever any of the parameters $\{\theta, u, t\}$ are varied.

As a consequence of not using the G^3 second shape factors, G^3 continuity of the approximation is no longer guaranteed. The method does still achieve G^2 continuity however, by construction. Whenever $|t - t_0| > 2d$ the G^3 shape

factors are used and hence the approximation will be G^3 continuous. The approximation method is therefore referred to as "G^{2+}" and is summarised below.

4.1 The Algorithm

The following steps summarise the approximation method:

1. Given a GCS, normalise it and transform $\{\kappa_0, \kappa_1, r\} \rightarrow \{\theta, u, t\}$ using (3), (6) and (8).
2. Check the parameters satisfy $|\theta| < \frac{\pi}{2}, |t| < \pi$ and $|u - \frac{1}{2}| < 0.4$.
3. Define the first shape factors as $\beta_1 = \frac{3}{2} - u$, $\gamma_1 = \frac{1}{2} + u$ from (10).
4. Calculate the second shape factors (β_2, γ_2) from (11) and (12).
5. The approximation is given by the quintic Bézier with control points defined in (4).

5 Analysis

This section aims to argue that, given any GCS curve within the specified bounds, the proposed approximation method will be acceptable (i.e. $\epsilon \leq 0.05$).

To begin consider the 3-dimensional C^0 function $\bar{\epsilon} : \mathbf{D} \subseteq \mathbb{R}^{\mathbf{3}} \rightarrow \mathbb{R}$ which maps the triplet $\{\theta, t, u\}$ to the error, ϵ, when approximated by the proposed method with the domain $\mathbf{D} = \{\mathbf{x} = (\theta, t, u) : [0, \frac{\pi}{2}] \times [0, \pi] \times [0.1, 0.9]\}$. Then for the proposed method to produce an acceptable approximation for every GCS within the bounds it must be shown that $\bar{\epsilon}(\mathbf{x}) \leq 0.05 \; \forall \mathbf{x} \in \mathbf{D}$.

The function $\bar{\epsilon}$ does not achieve C^1 continuity (see section 2.3) and thus partial derivatives are intractable. Analytic methods to calculate bounds are thus almost impossible. Instead sequential simplified approximations to $\bar{\epsilon}$ are considered. If the simplified approximations converge uniformly to $\bar{\epsilon}$ then in the limit the two functions, and thus the bounds of the functions, would coincide.

It is known that any C^0 function may be approximated by piecewise linear segments and the approximation will uniformly converge as the number of segments increase [11]. For a 3-dimensional C^0 function an analogous piecewise tri-linear segment approximation can be applied and will also converge uniformly as the number of tri-linear segments increase.

The approximations $\bar{\epsilon}_n$ of $\bar{\epsilon}$ are considered as its piecewise tri-linear interpolation. Each sequential approximation considers half the distance for each

one parameter linear segment and thus is defined on $(2^n + 1)^3$ lattice points (see Figure 6(a-b)).

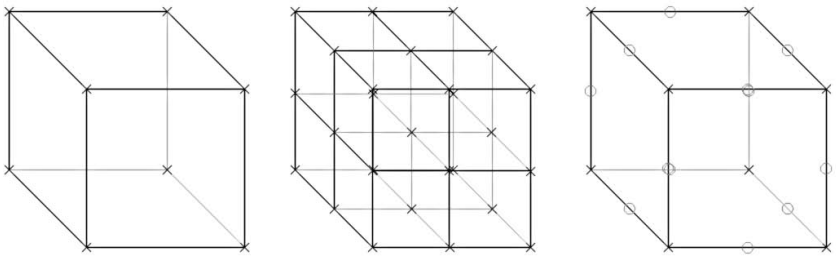

Figure 6: [a-b] Visualisation of the piecewise tri-linear interpolation (a) n=0, (b) n=1. [c] The cirles are considered for calculating the error of the tri-linear approximation.

Bounds for the function $\bar{\epsilon}_n$ can be easily calculated. Let the upper bound be denoted χ_n. This value is found from the maximum value of all lattice points, i.e. if $\mathbf{L}_n$ is the set of all lattice points then

$$\chi_n = \max_{\mathbf{x} \in \mathbf{L}_n} \{\bar{\epsilon}(\mathbf{x})\}.$$

For each sequential approximation an error value ξ_n, which represents an error of $\bar{\epsilon}_n$ to $\bar{\epsilon}$, can be generated. A comparison between the values of $\bar{\epsilon}$ and $\bar{\epsilon}_n$ at the midpoint of all neighbouring lattice points is considered (see Figure 6(c)). The error, ν_n, is then given from the largest difference between all those points. Thus if $\mathbf{N}_n$ is the set of all neighbouring lattice points then

$$\begin{aligned} \nu_n &= \max_{(\mathbf{x},\mathbf{y}) \in \mathbf{N}_n} \left\{ \bar{\epsilon}_n \left(\frac{\mathbf{x}+\mathbf{y}}{2} \right) - \bar{\epsilon} \left(\frac{\mathbf{x}+\mathbf{y}}{2} \right) \right\} \\ &= \max_{(\mathbf{x},\mathbf{y}) \in \mathbf{N}_n} \left\{ \frac{\bar{\epsilon}(\mathbf{x}) + \bar{\epsilon}(\mathbf{y})}{2} - \bar{\epsilon} \left(\frac{\mathbf{x}+\mathbf{y}}{2} \right) \right\}. \end{aligned}$$

From these values a bound for $\bar{\epsilon}$ can be estimated as $\xi_n = \chi_n + \nu_n$. In the limit as $n \to \infty$, $\nu_n \to 0$ and thus ξ_n tends towards the true bound of $\bar{\epsilon}$. The following table presents the data for $n = 0, \ldots, 7$:

From Table 1, the values of ξ_n appear to be tending to a value less than 0.05. Thus this data provides strong evidence that $\bar{\epsilon}(\mathbf{x}) \leq 0.05 \ \forall \mathbf{x} \in \mathbf{D}$ which would indicate that the proposed method produces an acceptable approximation for every GCS within the bounds.

n	$\lvert L_n \rvert$	χ_n	ν_n	ξ_n
0	2^3	0.025721	0.011702	0.037423
1	3^3	0.025721	0.009192	0.034913
2	5^3	0.025721	0.006524	0.032245
3	9^3	0.025721	0.003389	0.029110
4	17^3	0.025721	0.002040	0.027761
5	33^3	0.025721	0.001118	0.026839
6	65^3	0.025721	0.000546	0.026267
7	129^3	0.025721	0.000528	0.026249

Table 1: Table of bounds for sequential approximations of $\bar{\epsilon_n}$ to $\bar{\epsilon}$.

Furthermore, the values of ν_n are getting smaller as expected. This is because the sequential approximations of $\bar{\epsilon}_n$ are converging to $\bar{\epsilon}$. Most interestingly, the values for χ_n remain constant. This is because maximum value in the lattice was found at the boundary point $\bar{\epsilon}(\frac{\pi}{2}, \pi, 0.1)$ for all $n = 0, \ldots, 7$. This suggests that the upper bound is achieved at this point.

6 Examples

In this section examples of approximations to GCSs are given. The examples compare the proposed "G^{2+}" method with the G^3 method [8] (when $\beta_1 = \gamma_1 = 1$) and the quintic Hermite approximation [15]. The first example considers the GCS corresponding to the upper bound of $\bar{\epsilon}$, that is when $\{(\theta, t, u) = (\frac{\pi}{2}, \pi, 0.1)\}$ which has values of $\{(\kappa_0, \kappa_1, r) = (2.15, -1.00, -0.889)\}$.

From Figures 7 and 8 it is clear that the "G^{2+}" approximation outperforms both of the other methods when approximating this GCS. The error values for the three methods are $31\%, 29\%$ and 3%, for the Hermite, "G^3" and "G^{2+}" methods respectively.

Figure 9 demonstrates how the approximation performs across a variety of GCSs. For each plot the variation in the x-axis corresponds to a change in shape factor $0.1 < u < 0.9$. The variation in the y-axis corresponds to a change in the parameter $0 < t < \pi$. The winding angle is fixed to coincide with the bounding plane $\theta = \frac{\pi}{2}$ and the grey-scaled error ranges from white

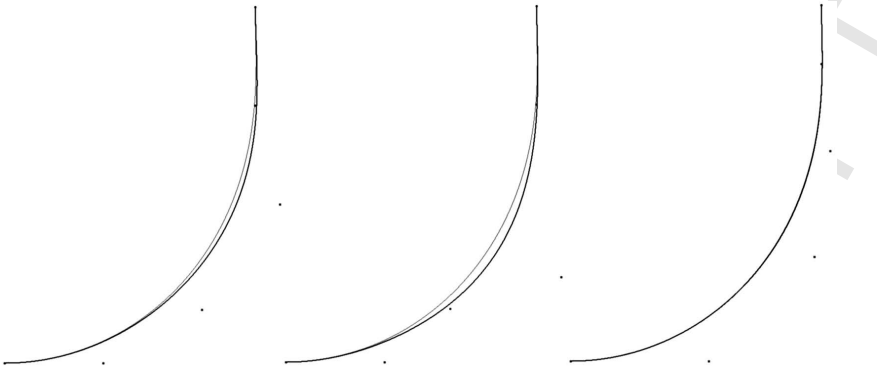

Figure 7: Approximations to the GCS $\{(\kappa_0, \kappa_1, r) = (2.15, -1.00, -0.889)\}$ [left - Hermite, middle - G^3, right - G^{2+}].

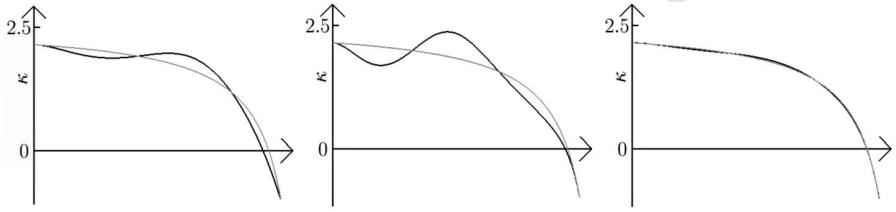

Figure 8: Curvature profiles of the approximations to the GCS $\{(\kappa_0, \kappa_1, r) = (2.15, -1.00, -0.889)\}$ [left - Hermite, middle - G^3, right - G^{2+}].

$(\epsilon = 0.00)$ to black $(\epsilon = 0.05)$.

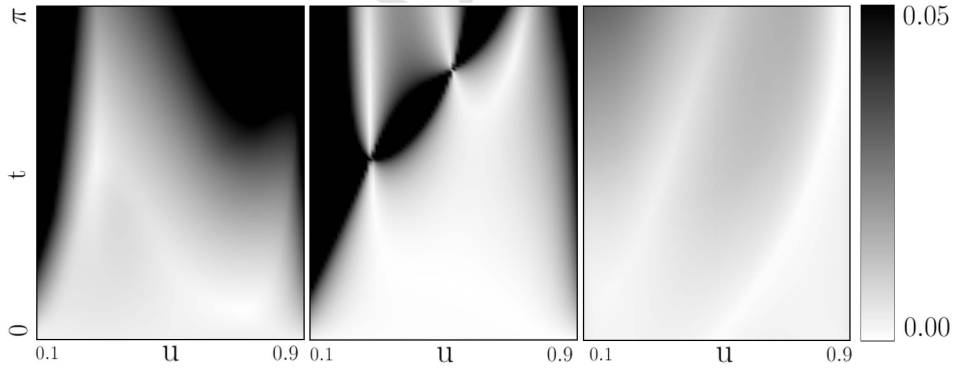

Figure 9: The error ϵ in the approximation methods [left - G^{2+}, middle - G^3, right - Hermite] when $\theta = \frac{\pi}{2}$.

It is clear from the figure that the "G^{2+}" approximation outperforms both of the other methods. The graph corresponding to"G^{2+}" does not contain any regions of unsatisfactory approximations whereas both the "G^3" and Hermite methods fail as t approaches π and as u approaches the boundaries $u = 0.1$ and $u = 0.9$.

The inflexibility of the Hermite method does not take into account the rising complexity of the shape of the GCS as t and u approach the boundary edges. The G^3 method appears to provide a better approximation except for the isolated regions in the upper center and upper right. These regions of unsatisfactory approximations correspond to denominator values approaching zero (see Figure 1). Furthermore, the method also fails as u approaches 0.1 and 0.9. This is a consequence of not varying the shape factors β_1, γ_1 as suggested by the numerical search (see (10)).

7 Conclusions

In this paper a method to approximate a GCS with a quintic Bézier curve is presented. The method builds upon the G^3 method described in [8] and is improved by removing the need for a numerical search thus reducing the computational cost of constructing an approximation. Furthermore, there is strong evidence that should the GCS be within certain bounds the method always yields an acceptable approximation within a tolerance of $\epsilon \leq 5\%$. Thus acceptable approximations can be formed without the need to calculate the computationally expensive error function.

The consequences of creating this deterministic approximation is more than just efficiency and robustness. The existence of this one-to-one mapping of a GCS with an acceptable approximation can be studied to infer characteristics of such approximations. These inferences can be drawn from the construction procedure and geometric properties of the GCS. This may eventually result in an approximation technique independent of the GCS itself. If the geometrical properties adhere exactly to a GCS then a high quality polynomial approximation is guaranteed. Following this reasoning, when the geometrical data does not correlate exactly to a GCS but is instead within a tolerance of a GCS, a high quality approximation can still be formed. This process of reverse engineering the GCS could lead to an efficient procedure for interpolating geometric data points with inherently fair polynomial curves.

A final problem to address is how to approximate a GCS if it lies outside the bounds. A proposed solution is to consider splitting the GCS into a sufficient amount of segments such that each segment lies within the specified bounds. Further work will consider how to subdivide the GCS in an

efficient way to guarantee an acceptable approximation with as few segments as possible.

8 Acknowledgements

The authors would like to thank the School of Mechanical Engineering at the University of Birmingham and Delcam PLC for providing financial support.

References

[1] Ali, J.M. Tookey, R.M. Ball, J.V. Ball, A.A. *The Generalised Cornu Spiral and its applications to span generation.* Journal of Computational and Applied Mathematics, (1994), p37-47.

[2] Farin, G. Rein, G. Sapidis, N.S. and Worsey, A.J. *Fairing Cubic B-Splines.* Computer Aided Geometric Design, Vol 4, (July 1986), p91-103.

[3] Rando, T. and Roulier, J.A. *Measures of Fairness for Curves and Surfaces.* Designing fair curves and surfaces, Society for Industrial and Applied Mathematics, Philadelphia, (1994), p75-122.

[4] Pal, T.K. and Nutbourne, A.W. *Two-dimensional curve synthesis using linear curvature elements.* Computer Aided Design, Vol 9, (April 1997), p121-134.

[5] Meek, D.S. and Walton, D.J. *Clothoid Spline Transition Spirals.* Mathematics of Computation, Vol 59, (July 1992), p117-133.

[6] Farin, G. *Curves and Surfaces for Computer Aided Graphical Design.* Academic Press (2002).

[7] Baumgarten, C. and Farin, G. *Approximation of Logarithmic Spirals.* Computer Aided Geometric Design, (1997), p515-532.

[8] Cross, B. and Cripps, R.J. G^3 *quintic polynomial approximation for Generalised Cornu Spiral segments.* Journal of Computational and Applied Mathematics 236, (2012), p3111-3122.

[9] Cripps, R.J. Hussain, M.Z. and Zhu, S. *Smooth polynomial approximation of spiral arcs.* Journal of Computational and Applied Mathematics 233, (2010), p2227-2234.

[10] Ling, C.C. Abbas, M. and Ali, J.M. *Approximating GCS by Low Energy Hermite Curve* European Journal of Scientific Research, Vol 46, No 4, (2010), p616-626.

[11] Cheney, E.W. *Approximation Theory*. Chelsea Publishing Company, Second Edition (1982).

[12] Dillen, F. *The Classification of Hypersurfaces of a Euclidean Space with Parallel Higher Fundamental Form*. Mathematische Zeitschrift 203 (1), (1990), p635-643.

[13] Guggenheimer, H.W. *Differential Geometry*. Dover Publications (1997).

[14] Wang, L.Z. Miura, K.T. Nakamae, E. Yamamoto, T. Wang, T.J. *An approximation approach of the clothoid curve defined in the interval* $[0, \pi/2]$ *and its offset by free-form curves*. Computer-Aided Design 33, (2001), p1049-1058.

[15] Sánchez-Reyes, J. and Chacón, J.M. *Polynomial approximation to clothoids via s-power series*. Computer Aided Design 35, (2003), p1305-1313.

[16] Press, W.H. Teukolsky, S.A. Vetterling W.T. Flannery B.P. *Numerical recipes in C, The art of scientific computing, Second edition* Cambridge University Press, (1994).

[17] Barsky, B.A. and DeRose, T.D. *Geometric Continuity of Parametric Curves: Three Equivalent Characterizations*. IEEE Computer Graphics & Applications, (November 1989), p60-68.

[18] Cripps, R.J. Ball, A.A. *Orthogonal C^2 Cubic Spline Curves* Geometrical Modeling and Computing: Seattle 2003, Nashboro Press (2004).